YITP-SB-11-21

The need for a local source of UHE CR nuclei

Andrew M. Taylor,[1] Markus Ahlers,[2] and Felix A. Aharonian[3, 4]

[1] *ISDC, Chemin d'Ecogia 16, Versoix, CH-1290, SWITZERLAND*
[2] *C.N. Yang Institute for Theoretical Physics, SUNY at Stony Brook, Stony Brook, NY 11794-3840, USA*
[3] *Dublin Institute for Advanced Studies, 5 Merrion Square, Dublin 2, IRELAND*
[4] *Max-Planck-Institut für Kernphysik, Postfach 103980, D-69029 Heidelberg, GERMANY*

Recent results of the Pierre Auger (Auger) fluorescence detectors indicate an increasingly heavy composition of ultra-high energy (UHE) cosmic rays (CRs). Assuming that this trend continues up to the highest energies observed by the Auger surface detectors we derive the constraints this places on the local source distribution of UHE CR nuclei. Utilizing an analytic description of UHE CR propagation we derive the expected spectra and composition for a wide range of source emission spectra. We find that sources of intermediate-to-heavy nuclei are consistent with the observed spectra and composition data above the ankle. This consistency requires the presence of nearby sources within 60 Mpc and 80 Mpc for silicon and iron only sources, respectively. The necessity of these local sources becomes even more compelling in the presence nano-Gauss local extragalactic magnetic fields.

PACS numbers: 13.85.Tp, 98.70.Sa

I. INTRODUCTION

Ultra-high energy CRs with energies above 10^{19} eV arrive at Earth with a frequency of less than one event per square-kilometer-year (*i.e.* with an energy flux of 30 eV cm^{-2} s^{-1}) in π steradian. The recently completed Pierre Auger observatory [1] with a surface detector covering an area of about 3000 km^2 is thus able to detect up to several hundred UHE CR events per year. However, due to the steeply falling CR spectrum the arrival frequency drops by about two orders of magnitude as we go up in energy by one decade, leaving only a few events per year detectable at energies around 10^{20} eV. Hence, the statistical uncertainty associated with the upper end of the spectrum is still large, limiting our knowledge of UHE CR composition and origin.

Before their arrival, UHE CRs must propagate across the astronomical distance between their source and Earth. The relevant interactions of UHE CR nuclei during propagation are Bethe-Heitler pair production and photo-disintegration in collisions with photons of the cosmic background radiation. The cross-sections of both these processes rise quickly above the threshold values of about 1 MeV and 10 MeV, respectively, in the nuclei's rest-frame. At even higher energies above 150 MeV pion production turns on and becomes the dominant energy loss process. However, for the UHE CR cutoff energies and composition we consider, which are motivated by the most recent Auger results, this process never plays a dominant role and may be safely neglected.

Provided the propagation time from their sources to Earth is greater than their energy loss time, UHE CRs invariably undergo these energy loss interactions. The break-up of nuclei via photo-disintegration produces lower mass nuclei with the same Lorentz factor. For heavy nuclei, the most dominant transitions are one-nucleon and two-nucleon losses. Secondary heavy nuclei remain close to the photo-disintegration resonance and quickly disintegrate further to lighter nuclei. Hence, on resonance, the initial mass composition of the sources is quickly shifted to lower values and in general shows a strong dependence on CR energy.

The arriving flux from an ensemble of UHE CR sources can be expected to contain suppression features at the high energies at which the photo-disintegration processes turn on and the nuclei particle's attenuation length decreases. Most prominently, for the case of a proton-dominated spectrum, the flux is expected to be suppressed by the *Greisen-Zatsepin-Kuz'min* (GZK) cutoff [2, 3] due to resonant pion photo-production interactions with the cosmic microwave background (CMB). Intriguingly, a suppression of the CR spectrum at about 5×10^{19} eV has been observed at a statistically significant level [4, 5]. However, since a similar feature may also appear in the spectrum from nuclei primaries, the observation of such a feature provides little clue as to the underlying composition. Such a suppression feature becomes a cutoff in the arriving flux if the attenuation length drops below the distance to the nearest UHE CR source. Thus, the shape of the suppression/cutoff feature does contain information about the source distribution, as has been investigated already for the case of UHE CR protons [6–8].

On their arrival at Earth, UHE CRs interact with molecules in the atmosphere and deposit their energy in the form of extensive air showers. The characteristics of these showers along the shower depth X (in g/cm^2) contain vital UHE CR composition information. On average, proton-induced showers reach their maximum development, $\langle X_{\rm max}\rangle$, deeper in the atmosphere than do showers of the same energy generated by heavier nuclei. Accompanying this effect, the shower to shower fluctuation of $X_{\rm max}$ about the mean, RMS($X_{\rm max}$), is larger

for proton-induced showers than for iron-induced showers of the same energy. As a result, measurements of both $\langle X_{\rm max}\rangle$ and RMS($X_{\rm max}$) can be used to infer the average chemical composition of the UHE CRs as a function of energy.

Auger has now released their first measurement results of RMS($X_{\rm max}$) [9, 10], along with those of $\langle X_{\rm max}\rangle$. These results seem to imply that the UHE CR spectrum contains a large fraction of intermediate or heavy mass nuclei, becoming increasingly heavy at high energies ($\sim 10^{19.5}$ eV). Furthermore, the small values of RMS($X_{\rm max}$) measured by Auger also imply that UHE CRs are composed of species with a relatively narrow distribution of charge at the highest measured energies, containing little or no protons or light nuclei. In this way, the new RMS($X_{\rm max}$) measurements not only confirm and reinforce the conclusions drawn from earlier average depth of shower maximum measurements, but also provide complementary information that enables one to constrain the distribution of the various chemical species present within the UHE CR spectrum.

Following our previous investigations into the composition of UHE CRs [11], a intermediate-heavy (silicon-to-iron) type composition was found to be motivated by the present complete Auger data set, with a hard ($\alpha < 2$) injection spectral index [31]. We here investigate further this result, in particular focusing on the local UHE CR source distribution inferred to exist if the observed trend in the composition continues up to highest energies observed by the ground array ($\sim 10^{20.2}$ eV). To aid this investigation we utilise an analytic description of UHE CR nuclei propagation already developed by the authors [12].

II. UHE CR NUCLEI FLUXES FROM A UNIFORM DISTRIBUTION OF SOURCES

With no prior knowledge about the UHE CR source population, a "universal" (homogeneous and isotropic) distribution is generally assumed. We adopt this assumption here as a means of investigating signatures of a departure from it. In order to quantify the effect of a different source distribution in this paper, we separate out the fluxes produced from source regions with shells of radii 0-3 Mpc, 3-9 Mpc, 9-27 Mpc, 27-81 Mpc, and 81-243 Mpc surrounding the Earth. In this way, the results obtained may be used to encapsulate the effects introduced by a non-"universal" local void of UHE CR sources.

We show in the upper-panel of Fig. 1 a breakdown of the total arriving flux from an ensemble of sources assuming they have a homogeneous distribution. These results have been obtained using both a Monte Carlo description of UHE CR nuclei propagation, whose details are described in Ref. [13], as well as an analytic description whose details are described below. An injection spectrum of $\alpha = 1.8$ and a maximum energy of

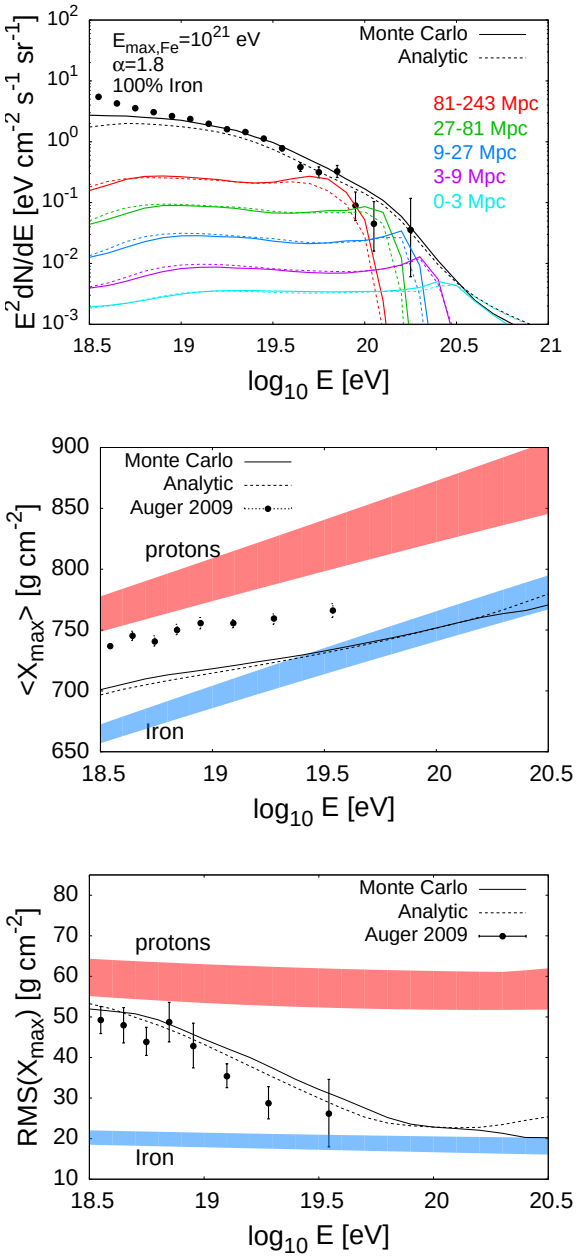

FIG. 1: **Top panel:** A breakdown of the arriving flux from shells of UHE CR Fe sources, obtained using a Monte Carlo description for UHE CR nuclei propagation. The results have been normalised to recent Auger measurements [14] at energies above 10^{19} eV. **Middle and bottom panels:** A comparison of the composition describing $\langle X_{\rm max}\rangle$ and RMS($X_{\rm max}$) values of the Monte Carlo and analytic descriptions. The hadronic model QGSJET 11 [15] has been adopted for these comparative calculations. The red and blue bands show the range of predictions of the $\langle X_{\rm max}\rangle$ and RMS($X_{\rm max}$) values for protons and iron, for various hadronic interaction models [15–18].

$E_{\rm Fe,max} = 10^{21}$ eV have here been assumed [32]. These

values were motivated by previous investigations into UHE CR nuclei sources [11]. From this figure, it is clearly seen that the arriving flux at the highest UHE CR energies ($E > 10^{20}$ eV) is dominated by the local source population.

In the middle and bottom panels of Fig. 1 the composition related information of the arriving flux, $\langle X_{\rm max}\rangle$ and RMS($X_{\rm max}$), are shown. For these results, the hadronic interaction model QGSJET 11 [15] has been adopted. The broad red and blue lines depicting the "proton" and "iron" values in these plots indicate the spread of predicted values from a range of hadronic interaction models [15–18].

To simplify the picture the effects of the presence of extragalactic magnetic fields on UHE CR propagation are neglected in this section. In section IV, these effects are incorporated to see how the field-free results in this section are altered.

The shape of the cutoff feature in the UHE CR spectrum carries in it valuable information about the local source distribution. A simple analytic description of this feature, found in Ref. [19], and developed further in [12], allows the different cutoffs in the fluxes from the various shells to be easily interpreted. To first order, photo-disintegration of heavy nuclei can be approximated by one-nucleon loss. The flux of nuclei with mass number A from a source at distance L with initial mass number $A_{\rm ini}$ follows simply,

$$\frac{N_A(E_A,L)}{N_{A_{\rm ini}}(E,0)} = \sum_{m=A}^{A_{\rm ini}} l_0 l_m^{A_{\rm ini}-1} e^{-\frac{L}{l_m}} \prod_{p=0(\neq m)}^{A_{\rm ini}} \frac{1}{l_m - l_p}\,. \quad (1)$$

Here, l_a denotes the interaction length of one-nucleon loss of the nucleus with mass number a. By employing (1), and summing over all possible mass numbers A (from 1 to $A_{\rm ini}$) different nucleon loss contribution functions for the flux from the source, the total nuclei flux from a single source is obtained,

$$\frac{{\rm d}N_{\rm total}(E,L)}{{\rm d}L} = \sum_{A=1}^{A_{\rm ini}} \frac{N_A(E_A,L)}{N_{A_{\rm ini}}(E_{A_{\rm ini}},0)}. \quad (2)$$

The agreement between the Monte Carlo and analytic results, seen in Fig. 1, demonstrates that for negligible (<pG) extragalactic fields the local source information (spectrum and composition) is essentially encapsulated by our simplified analytic model. Indeed, the different sets of photo-disintegration cross-sections used for the Monte Carlo and analytic descriptions, for which [20] and [21] have been used respectively, demonstrate further the robustness of these results. Using this analytic description, sets of models may be quickly scanned through in order to find the optimum set of injection index α, exponential energy cutoff $E_{\rm max}$ and source composition values able to "best-fit" the Auger results above 10^{19} eV.

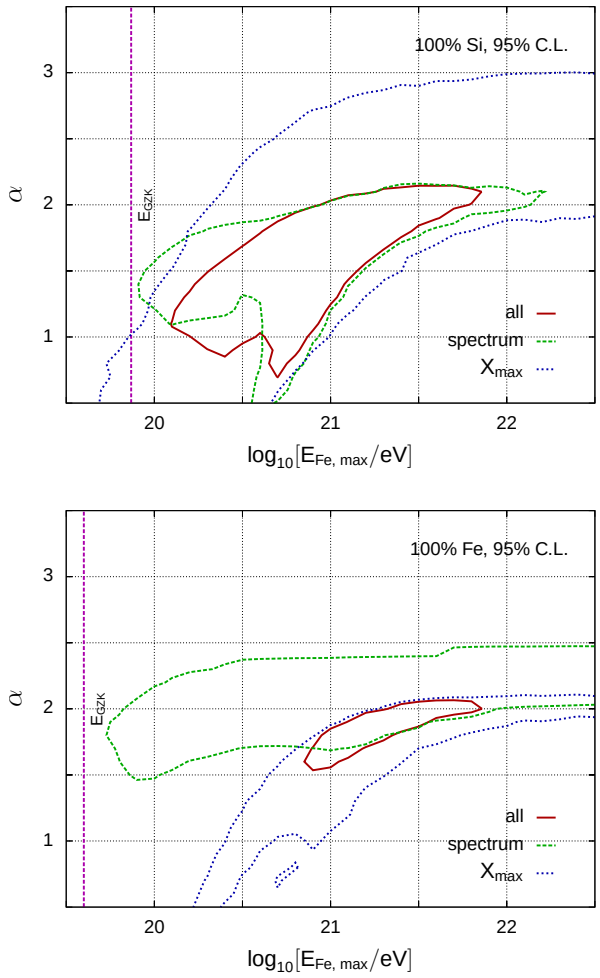

FIG. 2: Contour plots showing both the spectrum and $X_{\rm max}$ (ie. both $\langle X_{\rm max}\rangle$ and RMS($X_{\rm max}$)) goodness-of-fit results for silicon (upper panel) and iron (lower panel) source compositions. The spectral fits to the data have been carried out for energies above 10^{19} eV, and the QGSJET 11 hadronic model has been used as the hadronic model needed to obtain the theoretical $\langle X_{\rm max}\rangle$ and RMS($X_{\rm max}$) values.

Through the application of a goodness-of-fit (GOF) test, taking into account the systematic uncertainties in the measurement of CR energy, $\langle X_{\rm max}\rangle$, and RMS($X_{\rm max}$) (see Appendix A), we find that, in agreement with our earlier investigations [11], a intermediate-heavy composition ($A > 20$), hard spectral indices ($\alpha < 2$) and intermediate type cutoff energies ($E_{\rm Fe,max} \sim 10^{21}$ eV) are best able to describe the current data. Contour plots showing the "best-fit" regions for both silicon and iron only type sources are shown in Fig. 2. We also indicate in the plots the position of the GZK energy $E_{\rm GZK}$ in terms of $E_{\rm Fe,max}$. The fit to the data prefers considerably higher cutoff energies than the GZK energy. These plots demonstrate that both the spectra and composition information both provide new and differing constraints on the source spectral parameters, particularly for the case of heavy nuclei (iron) type sources.

III. THE EFFECT OF THE FINITE DISTANCE TO THE NEAREST SOURCE

The number density of local sources can not be much smaller than 10^{-5} Mpc^{-3} as can be estimated, *e.g.*, from the absence of "repeaters" in CR data [22, 23]. It is hence expected that the flux of CRs from sources much larger than a few 100 Mpc can be well approximated by a homogeneous distribution of sources. However, the finite (non-zero) distance to the nearest source of UHE CR nuclei leads to a breakdown of the homogeneous source distribution spectrum result at the highest energies, as already indicated in Fig. 1. We here demonstrate the effect introduced by this local void of UHE CR sources using both concrete examples as well as a statistical approach.

As an illustrative example, using typical "best-fit" model parameters motivated from our GOF results in the previous section, we show explicitly in Fig. 3 the alteration to the flux due to the failure of the homogeneous approximation. These results demonstrate the introduction of a very strong cutoff feature due to a non-zero distance to the first source, with this feature occurring at lower energy for intermediate nuclei such as silicon, than for heavy nuclei such as iron. It should be emphasised that the position (in energy) of the cutoff introduced by the distance to the nearest source is roughly independent of the spectral index (α) and cutoff energy ($E_{\rm Fe,max}$) of the primary spectrum. However, this result is only true when the source's maximum energy sits at energies much larger than the cutoff energy introduced by the local void of sources. We re-iterate here that these results rest on the assumption that the composition above energies where it has been measured ($10^{19.5}$ eV), continues to consist of intermediate-heavy nuclei up to the highest observed energy flux measurements ($10^{20.2}$ eV).

To put these results on a more general footing, we show in Fig. 4 the alteration to the GOF contour plots as the distance to the nearest source in increased. We find that for both silicon-only and iron-only source scenarios, the 99% C.L. undergoes a rapid decrease in size for minimum source distances in the range $9-27$ Mpc and $27-81$ Mpc respectively. Furthermore, for larger local voids, the remaining $E_{\rm Fe,max}$ values are larger than those typically considered feasible for candidate UHE CR sources. By imposing the constraint that the cutoff energy, $E_{\rm Fe,max}$, sits below 10^{22} eV, the subsequent upper limit on the source distance of 60 Mpc and 80 Mpc are found for silicon and iron type source respectively, at the 99% C.L. This reaffirms the result shown in Fig. 3, that a large $\gtrsim$81 Mpc local void in the source distribution would lead to difficulties in finding self-consistent fits to the spectral, $\langle X_{\rm max}\rangle$, and RMS($X_{\rm max}$) data of Auger.

We have assumed throughout this work so far that the extragalactic magnetic field strength is negligible. Though the overall flux from the *total* ensemble of shells

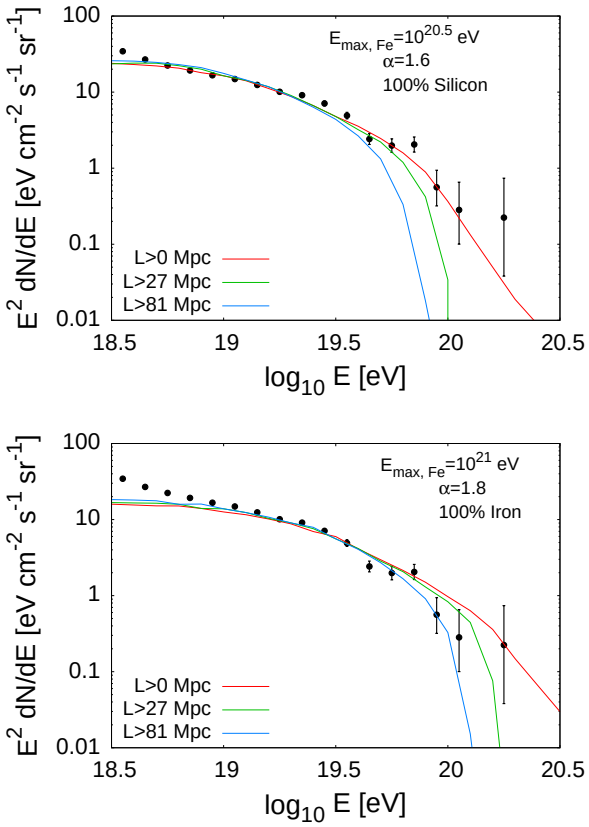

FIG. 3: The arriving UHE CR flux from a uniform distribution of UHE CR sources emitting a pure silicon (top), and pure iron (bottom) composition. A source spectral index (α) and cutoff energy ($E_{\rm Fe,max}$) of 1.6 and $10^{20.5}$ eV respectively for silicon and 1.8 and 10^{21} eV respectively for iron have been adopted, as motivated by our goodness-of-fit results in the previous section.

does not vary when an isotropic and homogeneous distribution of magnetic fields is introduced, the components arriving from different source shells will change. Furthermore, with an aim to investigate the possibility of a lack of nearby UHE CR sources, it is necessary that we take into account extragalactic magnetic field effects. In the following section we investigate these effects with the aim of making our conclusions more general.

IV. THE EFFECT OF EXTRAGALACTIC MAGNETIC FIELDS

In this section we investigate the effect these fields have on the arriving UHE CR flux and composition. In our calculations, the extragalactic magnetic field is always assumed to have a coherence length of 1 Mpc. Thus, within each of the magnetic patches (cells), the field contains a uniform component whose direction is assumed

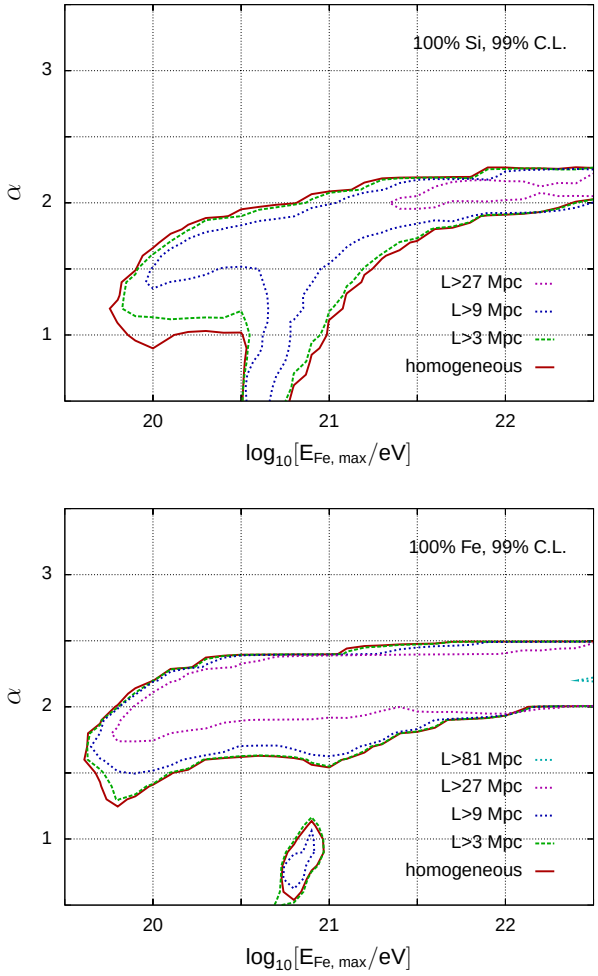

FIG. 4: Plots showing the disappearance of the 99% GOF contours as the distance to the first source is increased up to 81 Mpc.

to be orientated independently (randomly) to that of its corresponding orientation in the neighbouring cells. For particles with Larmor radii smaller than the magnetic patch coherence size (*e.g.* for iron nuclei with energies $\lesssim 10^{19}$ eV in a nG field), we assume a power law distribution of magnetic turbulence of the form $P(k) \propto k^{-q}$ (where $k = 2\pi/\lambda$), for which $q = 5/3$ corresponds to a Kolmogorov-type spectrum, $q = 3/2$ corresponds to a Kraichnan-type spectrum. This angular (and eventually spatial) diffusion of the particles is treated following a method very similar to that described in [8], which we refer to as the "delta-approximation" method (described in further detail in Appendix B). A Kolmogorov-type description of the magnetic field turbulence spectrum is assumed here. Ultra-high energy CRs in the simulation were considered to have arrived once they reached a distance of 100 kpc from Earth (this length scale being chosen to be smaller than both the corresponding particle loss length and gyro-radius).

Provided that a continuous distribution of sources exists on all scales, and that the magnetic fields are homogeneous and isotropic, extragalactic magnetic fields have no overall effect on the arriving flux [24]. However, since a minimum source distance scale must exist, a "magnetic horizon" is expected, with the flux from the nearby sources being prevented from arriving to us below a given energy [25]. Furthermore, the contribution of sub-"magnetic horizon" source shells can be increased by the presence of extragalactic magnetic fields, altering somewhat the flux arriving from the different source shells.

As seen in Fig. 5, the presence of extragalactic magnetic fields enhances the role played by local regions of sources on the arriving UHE CR flux. As envisaged from these results, and demonstrated in [26], a low energy cutoff of the arriving flux from distant shells of sources is introduced by the combined effect of a lack of local sources and the presence of non-negligible extragalactic magnetic fields. Below this cutoff energy, the UHE CR flux from even the nearest by sources is suppressed.

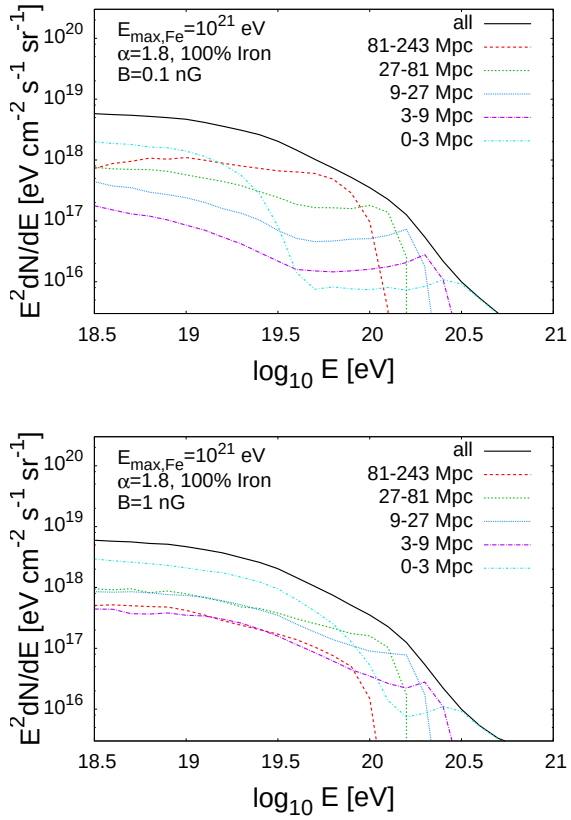

FIG. 5: A breakdown of the arriving flux from shells of UHE CR Fe emitting sources with an extragalactic magnetic field of strength (top) 0.1 nG and (bottom) 1 nG. Coherence lengths of 1 Mpc have been assumed for these calculations, which were obtained using a Monte Carlo description for UHE CR nuclei propagation.

Using the results shown in Fig. 5, the effect introduced

into the results of section III by the presence of a non-negligible (>pG) extragalactic magnetic field may be addressed. The dominant effect of these magnetic fields in combination with an absence of local sources is their alteration of the arriving composition, as demonstrated explicitly for 0.1 nG and 1 nG extragalactic magnetic fields in Fig. 6. Indeed, with a better handle on both the composition and distance to the nearest source, the composition may also provide a valuable probe of the local (intervening) extragalactic magnetic field.

V. SUMMARY

Following the motivation that UHE CRs consist of heavy nuclei, whose sources have been suggested to be local [27, 28], we have here looked closer at the requirements on their source distribution. In this work we obtained concrete quantitative constraints on the UHE CR source population. Making explicit use of the recently provided Auger spectral and shower composition results, along with detailed UHE CR nuclei modeling, we investigated whether consistency may be found with this data using single source composition models.

For the case of negligible extragalactic magnetic fields, we demonstrated that a simplified analytic description agrees well with the spectrum and composition results obtained from the complete Monte Carlo description. Utilising this analytic description, we made a scan over the source spectral index and exponential energy cutoff, for a given source composition, to obtain the goodness-of-fit contours. We found that hard ($\alpha < 2$) source spectral indices and intermediate cutoff energies ($E_{\rm Fe,max} \sim 10^{20.5} - 10^{21}$ eV) for intermediate-to-heavy nuclei could provide a good fit to the full set of Auger UHE CR measurements above 10^{19} eV.

Through the consideration of shells of UHE CR sources, we investigated the proximity of the UHE CR nuclei sources required if the presently observed trend of an increasingly heavy composition continues up to the highest energies observed by the ground array ($10^{20.2}$ eV). By varying the size of the local void up to the nearest source, we investigated how detrimental the effect of this was on the goodness-of-fits contours. Provided that the sources maximum energy lay below 10^{22} eV, we found that the nearest sources had to be within 60 Mpc and 80 Mpc for silicon and iron only sources respectively.

If, however, extragalactic magnetic fields are sufficiently strong (>pG), the arriving flux from the different nuclei source shells is altered considerably. Though this effect is weakest at the highest energies, a local void of sources scenario with such an intervening field, may alter the arriving flux at energies below the cutoff feature, and thus alter the goodness-of-fit contour landscapes obtained in Fig. 2. However such (<nG strength) fields are found to be unable to alter significantly our upper bound on the nearest source distance.

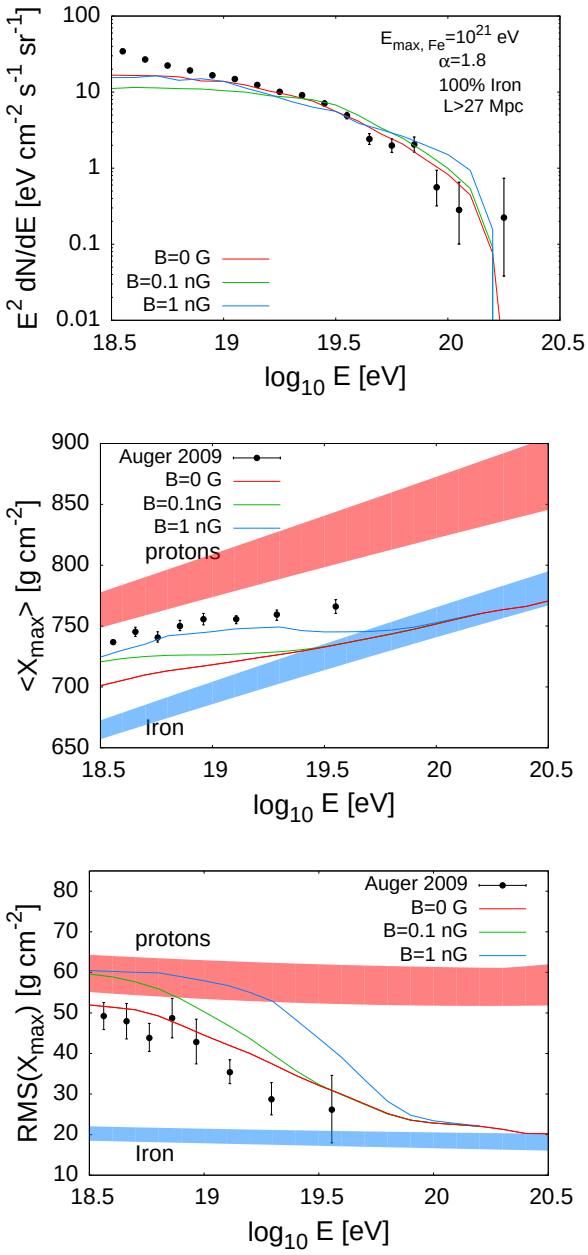

FIG. 6: The combined effect on the iron spectrum (top panel) and composition (middle and bottom panel) due to a local (L> 27 Mpc) void of sources and a non-negligible extragalactic magnetic field (0.1 and 1 nG).

Our results demonstrate that exciting consequences follow from the intermediate-to-heavy nuclei component uncovered by Auger measurements. With nuclei photodisintegration inevitably occurring during propagation, tough constraints are placed on the source proximity and environment. Furthermore, future Auger spectral

and composition measurements are anticipated to soon tighten these constraints. With few candidate sources within the present upper bound distance suggested (< 60-80 Mpc), the puzzle as to the UHE CR origin both remains and becomes even more intriguing.

Acknowledgments

AMT acknowledges support by the Swiss National Science Foundation grant PP00P2 123426. MA acknowledges support by the US National Science Foundation Grant No PHY-0969739 and by the Research Foundation of SUNY at Stony Brook.

Appendix A: Goodness-of-Fit Test

We perform a goodness of fit (GOF) test of the compatibility of the Auger data with a given model following Ref. [29]. For a fixed source composition of nuclei we vary the universal spectral index α of the emission spectrum and the maximal rigidity cutoff $E_{\rm Fe,max}$, described in [31] and [32].

Given the acceptance A_n (in units of area per unit time per unit solid angle) of the experiment in bin n centered at energy E_n with bin width Δ_n, the number of expected events is

$$\mu_n(\alpha, E_{\rm Fe,max}, \mathcal{N}, \delta_E) = A_n \mathcal{N} \int_{E_n^-}^{E_n^+} {\rm d}E \sum_i \frac{{\rm d}N_i}{{\rm d}E}(E)\,, \quad \text{(A1)}$$

where ${\rm d}N_i/{\rm d}E$ is the flux of nuclei Z arriving at the detector and the boundaries are $E_n^\pm = E_n(1+\delta_E) \pm \Delta_n/2$. The parameter δ_E in Eq. (A1) is a fractional energy-scale shift that takes into account the uncertainty in the energy-scale and $\mathcal{N}$ is the normalization of the source luminosity.

A fraction ϵ_n of the expected μ_n events per bin passes the quality cuts for the distribution of shower maxima X. This distribution is only known by its first two moments, the average shower maximum $\langle X\rangle_n$ and its root-mean-square (RMS) ΔX_n [9]. For the GOF we hence divide the distribution of shower maxima X into three intervals $(X_{m,n}^-, X_{m,n}^+)$, such that each interval contains 1/3 of the total number of observed events. For a Gaussian distribution this corresponds to a central bin of size $X_{0,n}^\pm \simeq \langle X\rangle_n(1+\delta_{\langle X\rangle}) \pm 0.43\Delta X_n(1+\delta_{\rm RMS}))$ and two bins containing all other events left ($m=-1$) and right ($m=1$) to it. Here, we introduce the fractional uncertainties $\delta_{\langle X\rangle}$ and $\delta_{\rm RMS}$ of the mean and RMS of the shower maximum, respectively.

We emphasise that the binning method of the shower maxima that we employ can only as an approximation. As a check of this approach we try to reconstruct $\langle X\rangle$ and ΔX from this X-binning by a simple χ^2-fit. The number of events passing the quality cuts is known from Fig. 2 of Ref. [9]. Figure 7 shows the reconstructed 1σ contours in comparison to the statistical uncertainty of the measurement extracted from Fig. 2 and 3 of Ref. [9]. The contours are consistent with the data and reproduce the right order of magnitude of the statistical uncertainty.

The predicted distribution of shower maxima can be determined by hadronic interactions models such as QGSJET 11 [15]. We assume in the following that the distribution in the n-th energy bin can be approximated by a Gaussian distribution with mean X_n and RMS σ_n. The expected number of events in the X sub-bins $m=-1,0,1$ is hence of the form

$$\mu_{m,n}(\alpha, E_{\rm Fe,max}, \mathcal{N}, \delta_E, \delta_{\langle X\rangle}, \delta_{\rm RMS}) = \epsilon_n \mu_n(\alpha, E_{\rm Fe,max}, \mathcal{N}, \delta_E) \int_{X_{m,n}^-}^{X_{m,n}^+} {\rm d}X \, \frac{e^{-\frac{(X-X_n)^2}{2\sigma_n^2}}}{\sqrt{2\pi}\sigma_n}\,. \quad \text{(A2)}$$

The probability $P_n(N_{{\rm tot},n})$ of observing $N_{{\rm tot},n}$ events in the n-th energy bin follows a Poisson distribution $f(N_{{\rm tot},n}, \mu_n)$ with mean μ_n. The $\epsilon_n N_{{\rm tot},n}$ events passing the quality cuts distribute between the three X-bins following a Poisson distribution with mean $\mu_{m,n}$ subject to the constraint $\epsilon_n N_{{\rm tot},n} = N_{-1,n} + N_{0,n} + N_{1,n}$. The conditional probability is

$$P_n'(N_{-1,n}, N_{0,n}, N_{1,n}) = \frac{f(N_{-1,n}, \mu_{-1,n}) f(N_{0,n}, \mu_{0,n}) f(N_{1,n}, \mu_{1,n})}{f(\epsilon_n N_n, \epsilon_n \mu_n)}\,. \quad \text{(A3)}$$

Hence the total probability of observing a set of events $\{N\}$ is given as

$$P(\{N\}; \alpha, E_{\rm Fe,max}, \mathcal{N}, \delta_{\langle X\rangle}, \delta_{\rm RMS}, \delta_E) = \prod_n P_n(N_{\rm tot,n}) \prod_\ell P_\ell'(N_{-1,\ell}, N_{0,\ell}, N_{1,\ell})\,. \quad \text{(A4)}$$

Here the first product runs over all energy bins used for the CR spectrum and the second product runs over all bins where additional information about the elongation rate distribution is available.

As a next step we marginalize over the experimental systematic uncertainty in the energy scale δ_E, shower maximum $\delta_{\langle X\rangle}$ and root-mean-square $\delta_{\rm RMS}$ as well as the normalization $\mathcal{N}$. We assume a flat prior with $|\delta_E| < 20\%$, $|\delta_{\langle X\rangle}| < 2\%$ and $|\delta_{\rm RMS}| < 10\%$. Marginalization is done by maximizing the probability of the actual experimental observation. We hence define

$$\widehat{P}(\{N\}; \alpha, E_{\rm Fe,max}) \equiv P(\{N\}; \alpha, E_{\rm Fe,max}, \widehat{\mathcal{N}}, \widehat{\delta}_{\langle X\rangle}, \widehat{\delta}_{\rm RMS}, \widehat{\delta}_E)\,, \quad \text{(A5)}$$

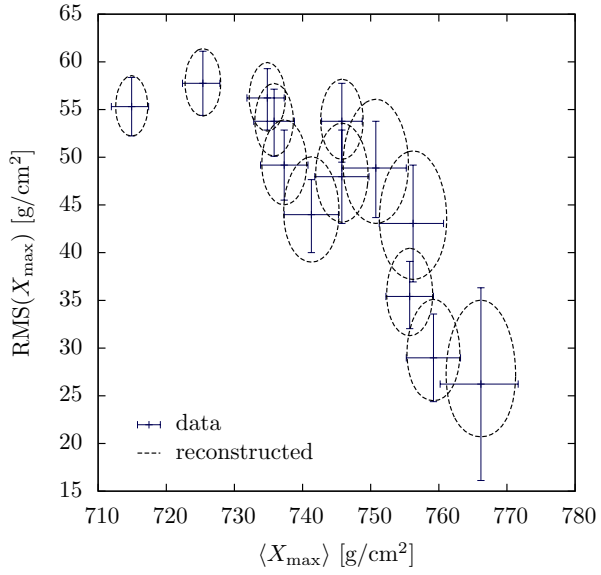

FIG. 7: The statistical uncertainty of the measured mean and RMS of the shower maximum from Ref. [9] compared to the uncertainty of the reconstruction from the three X-bins introduced for the goodness of fit.

where the set of parameters $\{\widehat{\mathcal{N}}, \widehat{\delta}_{\langle X\rangle}, \widehat{\delta}_{\rm RMS}, \widehat{\delta}_E\}$ maximizes the probability (A5) for the experimental result $\{N^{\rm exp}\}$, consisting of the total events per bin $N^{\rm exp}_{{\rm tot},n}$ as well as $N^{\rm exp}_{m,n} = \epsilon_n N^{\rm exp}_{{\rm tot},n}/3$, if available, which follows from the construction of the X-binning. In the marginalization procedure we also impose a prior on the normalization $\mathcal{N}$ by requiring that the model spectra do not exceed the Auger data below the first bin used in the fit by more than three standard deviations.

Finally, the model $(\alpha, E_{\rm Fe,max})$ is compatible with the experimental results at a given GOF if

$$\sum_{\widehat{P}(\{N\})>\widehat{P}(\{N^{\rm exp}\})} \widehat{P}(\{N\};\alpha, E_{\rm Fe,max}) \leq {\rm GOF}\,. \qquad \text{(A6)}$$

Technically, this calculation is performed by generating a large number $\{N^{\rm rep}\}$ of replica experiments following the probability distribution (A5) and by imposing that a fraction F with $\widehat{P}(\{N^{\rm rep}\}) > \widehat{P}(\{N^{\rm exp}\})$ satisfies $F \leq$ GOF.

Appendix B: A Simplified Description for UHE CR Propagation Through Turbulent Fields

We here describe the results of an investigate we carried out comparing two different descriptions for the diffusive propagation process of UHE CR in turbulent magnetic fields.

As discussed in [30], a turbulent field may be generated by adding plane waves whose amplitudes are dictated by the magnetic power spectrum,

$$\boldsymbol{B} = \sum_n \delta\boldsymbol{B}_n \qquad \text{(B1)}$$

where $\delta\boldsymbol{B}_n = \boldsymbol{\xi_n} A_n e^{\left(ik_n x' + \phi_n\right)}$, with $x' = x\cos\alpha - y\sin\alpha$, α describing the orientation of the wave (randomly chosen), $\boldsymbol{\xi_n}$ describing the (randomly chosen) polarisation of the wave (ie. over each wavelength $\boldsymbol{\xi_n}$ describes an ellipse in the $y'-z'$ plane), A_n describing the amplitude of the wave, k_n $(= 2\pi/\lambda_n)$ describing the wavenumber, and ϕ_n is a random phase. The amplitudes of the different waves are given a power law distribution of the form $A_n \propto k_n^{-q/2}$. For the purpose of our comparison we assume a Kolmogorov spectrum (*i.e.* $q = 5/3$).

We prepare a turbulent magnetic field region, containing an ensemble of waves with wavelengths between $\lambda_{\rm min}$ and $\lambda_{\rm max}$. It is assumed that a guiding mean-field, B_0, lies along the z-direction, and that the sum of the energy within the turbulent field is equal to the total energy within the guiding field ($B_0^2 = \sum_n \delta B_n^2$). We describe the turbulence using 50 isotropic waves, with 10 waves per decade (*i.e.* $\lambda_{\rm max}/\lambda_{\rm min} = 10^5$). The Bulirsch-Stoer method was used to track the particles in the field.

A simplified description of turbulent propagation, however, may also be obtained through a scattering description of UHE CR interaction with the turbulent field. In this description, UHE CR stochastically interact with scattering centers whose density is dictated by the energy density in the turbulence power spectrum at the wavelength matching the gyro-radius of the UHE CR. We refer to this description as the "delta-approximation" case, since it assumes only resonant scattering. The resonant scattering angle of this process is given by

$$\Delta\theta = \begin{cases} 1 & R_{\rm L} < L_{\rm coh}\,, \\ \frac{L_{\rm coh}}{R_{\rm L}} & R_{\rm L} > L_{\rm coh}\,, \end{cases} \qquad \text{(B2)}$$

where $R_{\rm L}$ is the particle's Larmor radius and $L_{\rm coh}$ is the magnetic field's coherence length. The corresponding scattering length is then given by

$$R_{\rm scatt}(\Delta\theta) = aL_{\rm coh} \begin{cases} \left(\frac{R_{\rm L}}{L_{\rm coh}}\right)^{2-q} & R_{\rm L} < L_{\rm coh}\,, \\ 1 & R_{\rm L} > L_{\rm coh}\,, \end{cases} \qquad \text{(B3)}$$

where the factor a describes how far this scattering is from the Bohm regime (*i.e.* $a = 1$ at the Bohm limit, giving rise to approximately one scattering per gyro-radius) for particles whose gyro-radii are at the scale $\lambda_{\rm max}$. The factor $(2-q)$ may be thought to describe the exponent in the energy dependence of the density of (resonant turbulence) scatterers. In order to scale down this result to allow us to probe the low angle scattering regime, we employ a small angle scattering length of size $\delta\theta$, $R_{\rm scatt}(\delta\theta) = (\delta\theta/\Delta\theta)^2 R_{\rm scatt}(\Delta\theta)$.

We compare the growth of spread of particles in the mean-field direction (Δz) as a function of time for both

the simplified description and that of the full turbulent field description in Fig. 8, for the case of $a = 1$. For this simulation, the particles were all started from the same position in the static turbulent field with an isotropic distribution of directions.

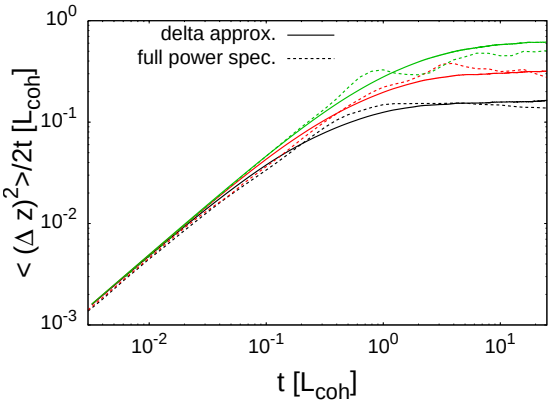

FIG. 8: A plot comparing the spreading of particles along the mean-field direction during propagation for both the full turbulent field description and the simplified "delta-approximation". These results were obtained for 10^{18} eV energy UHECR iron nuclei in 0.1 nG, 1 nG, and 10 nG extragalactic magnetic field with a 1 Mpc coherence length.

With good agreement found between the "full power spectrum" and the "delta-approximation" descriptions we conclude that the "delta-approximation" method is able to provide an accurate description for UHE CR propagation in extragalactic magnetic fields.

[1] J. Abraham *et al.* [Pierre Auger Collaboration], Nucl. Instrum. Meth. A **523** (2004) 50.
[2] K. Greisen, Phys. Rev. Lett. **16**, 748 (1966).
[3] G. T. Zatsepin and V. A. Kuz'min, JETP Lett. **4**, 78 (1966) [Pisma Zh. Eksp. Teor. Fiz. **4**, 114 (1966)].
[4] R. Abbasi *et al.* [HiRes Collaboration], Phys. Rev. Lett. **100**, 101101 (2008) [arXiv:astro-ph/0703099].
[5] J. Abraham *et al.* [Pierre Auger Collaboration], Phys. Rev. Lett. **101**, 061101 (2008) [arXiv:0806.4302 [astro-ph]].
[6] A. M. Taylor and F. A. Aharonian, Phys. Rev. D **79** (2009) 083010 [arXiv:0811.0396 [astro-ph]].
[7] V. Berezinsky, A. Z. Gazizov and S. I. Grigorieva, Phys. Rev. D **74** (2006) 043005 [arXiv:hep-ph/0204357].
[8] F. A. Aharonian and J. W. Cronin, Phys. Rev. D **50** (1994) 1892.
[9] J. Abraham *et al.* [Pierre Auger Observatory Collaboration], Phys. Rev. Lett. **104** (2010) 091101 [arXiv:1002.0699 [astro-ph.HE]].
[10] M. Unger and f. t. P. Collaboration, arXiv:1103.5857 [astro-ph.HE].
[11] D. Hooper and A. M. Taylor, Astropart. Phys. **33** (2010) 151 [arXiv:0910.1842 [astro-ph.HE]].
[12] M. Ahlers and A. M. Taylor, Phys. Rev. D **82** (2010) 123005 [arXiv:1010.3019 [astro-ph.HE]].
[13] D. Hooper, S. Sarkar and A. M. Taylor, Astropart. Phys. **27** (2007) 199 [arXiv:astro-ph/0608085].
[14] J. Abraham *et al.* [The Pierre Auger Collaboration], arXiv:0906.2189 [Unknown].
[15] S.S. Ostapchenko, Nucl. Phys. Proc. Suppl. **151** (2006), 143
[16] N.N. Kalmykov and S.S. Ostapchenko, Phys. Atom. Nucl. **56** (1993), 346; S.S. Ostapchenko, Nucl. Phys. Proc. Suppl. **151** (2006), 143; N. N. Kalmykov, S. S. Ostapchenko and A. I. Pavlov, Nucl. Phys. Proc. Suppl. **52B**, 17 (1997).
[17] E. J. Ahn, R. Engel, T. K. Gaisser, P. Lipari and T. Stanev, arXiv:0906.4113 [hep-ph]; R. S. Fletcher, T. K. Gaisser, P. Lipari and T. Stanev, Phys. Rev. D **50**, 5710 (1994).
[18] T. Pierog and K. Werner, Phys. Rev. Lett. **101** (2008), 171101; K. Werner and T. Pierog, AIP Conf. Proc. **928**, 111 (2007) [arXiv:0707.3330 [astro-ph]].
[19] D. Hooper, S. Sarkar and A. M. Taylor, Phys. Rev. D **77** (2008) 103007 [arXiv:0802.1538 [astro-ph]].
[20] E. Khan *et al.*, Astropart. Phys. **23** (2005) 191.
[21] A. J. Koning, S. Hilaire and M. C. Duijvestijn, EDP Sciences, 2008, p. 211-214.
[22] P. Blasi and D. De Marco, Astropart. Phys. **20** (2004) 559 [arXiv:astro-ph/0307067].
[23] T. Kashti and E. Waxman, JCAP **0805**, 006 (2008) [arXiv:0801.4516 [astro-ph]].
[24] R. Aloisio and V. Berezinsky, Astrophys. J. **612** (2004) 900 [arXiv:astro-ph/0403095].
[25] M. Lemoine, Phys. Rev. D **71** (2005) 083007 [arXiv:astro-ph/0411173].
[26] N. Globus, D. Allard and E. Parizot, arXiv:0709.1541 [astro-ph].
[27] T. Wibig and A. W. Wolfendale, arXiv:0712.3403 [astro-ph].

[28] T. Piran, arXiv:1005.3311 [astro-ph.HE].
[29] M. Ahlers, L. A. Anchordoqui, M. C. Gonzalez-Garcia, F. Halzen and S. Sarkar, Astropart. Phys. **34**, 106 (2010) [arXiv:1005.2620 [astro-ph.HE]].
[30] J. Giacalone and J. R. Jokipii, 1994ApJ...430L.137G
[31] This spectral index refers to an injection spectrum of the form $\mathrm{d}N/\mathrm{d}E \propto E^{-\alpha}$
[32] This maximum energy refers to the charge-dependent exponential cutoff energy, $\mathrm{d}N/\mathrm{d}E \propto E^{-\alpha} e^{-E/E_{Z,\max}}$, where $E_{Z,\max} = (Z/26) \times E_{\mathrm{Fe,max}}$